Wind fluctuations affect the mean behaviour of naturally ventilated systems

Wind fluctuations affect the mean behaviour of naturally ventilated systems

Riccardo Vesipa[a], Luca Ridolfi[a], Pietro Salizzoni[b]

[a]*DIATI, Politecnico di Torino, C.so Duca degli Abruzzi 24, 10129, Torino, Italy*
[b] *Laboratoire de Mécanique des Fluides et d'Acoustique, University of Lyon, CNRS UMR 5509 Ecole Centrale de Lyon, INSA Lyon, Université Claude Bernard, 36, avenue Guy de Collongue, 69134 Ecully, France.*

Abstract

We study the dynamics of a naturally ventilated room in which a point source provides a steady source of buoyancy and which is affected by an opposing unsteady wind. The wind is modelled as a stochastic forcing, which aims at simulating realistic velocity fluctuations as observed in the lower atmosphere. Our main finding is the occurrence of a "noise-induced transition", namely a structural change of the mean behaviour of the system: the warm-cold air interface does not fluctuate around the elevation exhibited when wind is constant, but oscillations occur around a new (significantly lower) interface elevation. We provide the physical explanation for such a counter-intuitive behaviour and show its dependence on (i) wind characteristics (intensity and timescale of fluctuations) and (ii) relative strength of wind over thermal loads. A realistic example case shows that the behaviour highlighted here has potentially major implications in the design and management of naturally ventilated buildings.

Keywords: natural ventilation, wind fluctuations, noise-induced phenomena, multistability, stochastic dynamics
2010 MSC: 00-01, 99-00

Nomenclature

Latin letters

A_c	Cross-sectional area of the room
A_B	Cross-sectional area of the bottom opening
A_T	Cross-sectional area of the top opening
B_0	Strength of the point-source of buoyancy
B	Buoyancy of the warm layer
C	Coefficient for turbulent entrainment in plumes
C_{pl}	Wind pressure coefficient for the lower opening
C_{pu}	Wind pressure coefficient for the upper opening
$C_{V,wv}$	Coefficient of variation of the wind velocity
g	Gravitational acceleration
g'	Reduced gravity or buoyancy of the buoyant layer
$g'(z)$	Reduced gravity of the plume at elevation z
g'_H	Reduced gravity of the plume at the ceiling ($z = H$)
g'_P	Reduced gravity of the plume at cold-warm interface ($z = h$)
g'_0	Reduced gravity of the buoyant layer at equilibrium
h	Elevation above the floor of the interface between the cold air and the warm layer
h_0	Elevation of the interface at equilibrium
H	Height of the room
Q_P	Flow rate of the plume at cold-warm interface ($z = h$)
$Q_P(z)$	Flow rate of the plume at elevation z
$Q_{T,w,\max}$	Maximum flow through the top opening induced by wind
$Q_{T,b,\max}$	Maximum flow through the top opening induced by buoyancy forces
Δp_b	Pressure difference between upwind and downwind facades induced by buoyancy forces
Δp_w	Pressure difference between upwind and downwind facades induced by wind
$\mathcal{P}$	Parameter that quantifies the strength of the buoyancy forces over the wind forces
t	Time
T_{Bf}	Filling box time
v	Wind velocity
$v(t)$	Time-dependent wind velocity
v_0	Mean wind velocity
$v'(t)$	Wind velocity fluctuations
V	Vent parameter
W	Wind parameter
$W(t)$	Time varying wind parameter
W_0	Mean wind parameter
ΔW	Sudden variation of the wind parameter
z	Upward vertical axis starting from the point-source of buoyancy

Greek letters

$\gamma(t)$	Parameter that quantifies the deviation of the reduced gravity of the buoyant layer from equilibrium condition (=1 at equilibrium)
γ_{eq}	Average reduced gravity attained during the dynamical equilibrium phase
$\eta(t)$	Parameter that quantifies the deviation of the interface elevation of the buoyant layer from equilibrium conditions (=1 at equilibrium)

*Corresponding author
Email address: riccardo.vesipa@polito.it (Riccardo Vesipa)

Wind fluctuations affect the mean behaviour of naturally ventilated systems

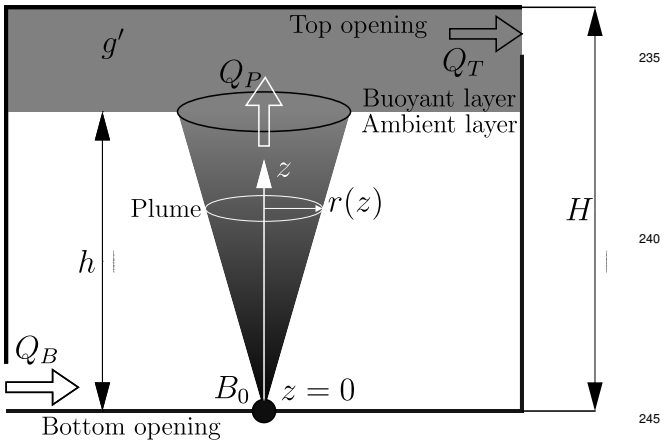

Figure 1: The naturally ventilated system considered in this study. It consists of a room with a single point-source of buoyancy that generates an ascending thermal plume (shaded in grey). In case of no (or weak) wind, a stratification takes place and a warm buoyant layer forms above the cold ambient air. Ventilation occurs through the top (warm air outlet) and bottom (fresh air inlet) openings.

where $g' = g\Delta\rho/\rho$ is referred to as the "reduced gravity" (g is the gravitational acceleration), $C = (6\alpha/5)(9\alpha\pi^2/10)^{1/3}$, with $\alpha \simeq 0.1$ a reference value for the turbulent entrainment coefficient of the thermal plume [41].

The warm buoyant layer induces a pressure difference (at $z = H$) equal to $\Delta p_b = \rho g'(H - h)$ (the subscript "b" stands for "buoyancy") that in turn produces a stack effect driving the room ventilation.

Due to volume conservation within the room, in steady state conditions, the net flow rate through all opening is zero, namely $Q_B = -Q_T$. It follows that the flow through each opening depends on the characteristics of both openings, and the flow (positive when directed from the inside to the outside of the room) through the top opening is [7, 17]

$$Q_{T,b} = +A^*[g'(H - h)]^{1/2}, \tag{3}$$

where

$$A^* = \frac{\sqrt{2}c_B A_B c_T A_T}{\sqrt{c_B^2 A_B^2 + c_T^2 A_T^2}}, \tag{4}$$

is the "effective opening area" [2].

The presence of wind can radically modify this picture, as it induces a further forcing on the system due to a pressure difference between the building facades, determined as [40]

$$\Delta p_w = \frac{1}{2}\rho\left(C_{pu} - C_{pl}\right)v^2, \tag{5}$$

where v is the wind velocity (subscript w stands for "wind"), and C_{pl} and C_{pu} are the wind pressure coefficient for the lower and upper openings, respectively. These wind pressure coefficients depend to a great extent on the location of openings, building shape, and architectonic details [8]. These coefficients should therefore be selected with caution.

The wind can either assist or contrast the natural ventilation of the room. In the case of an assisting wind (i.e., the top opening is in the downwind wall) the interface elevation of the warm layer h moves towards a higher level. In the case of an opposing wind (the top opening is in the upwind wall), the picture is more complex. Three flow regimes can be observed [17]:

- in the "stratified forward flow" (regime $\mathcal{A}$ in Fig. 2a), the wind is not strong enough to overcome the stack effect. Wind reduces the outflow through the top opening, thus reducing the amount of fresh air that enters from the bottom opening and inducing h to move towards a lower level;
- in the "stratified reverse flow" (regime $\mathcal{B}$ in Fig. 2b), the wind overcomes the stack effect and the flow through the top opening is reversed. Ambient air intrudes from the top opening in the warm buoyant layer, the flow through the bottom opening is from inside to outside, and no fresh air enters to ventilate the room. However, the warm buoyant layer is preserved, even thought h moves towards progressively lower levels. Regime $\mathcal{B}$ cannot persist over time. If wind reduces, the system goes back to regime $\mathcal{A}$. If wind persists, h reaches the floor and regime C arises.
- in the "mixed reverse flow" (regime C in Fig. 2c), fresh ambient air is driven by the wind through the top opening and mixes perfectly with the warm air from the buoyancy source. The flow through the bottom opening is from inside to outside. No warm buoyant layer exists and $h = 0$.

In order to model the transient dynamics of a ventilated room in the case of an opposing wind, a set of two coupled equations (that express the conservation of buoyancy and volume) is required. A different set of equations is adopted to model the dynamics of the regimes $\mathcal{A}, \mathcal{B}$ and C. The choice of the appropriate set is based on the parameter [17]

$$\mathcal{P} = [g'(H - h)] - \Delta p_w/\rho \tag{6}$$

that quantifies the strength of the buoyancy forces (stack effect) over the wind forces.

When $\mathcal{P} > 0$, buoyancy dominates over wind. The flow at the top opening is from inside to outside and reads $Q_T = +A^*\left\{[g'(H - h) - \Delta p_w/\rho]^{1/2}\right\}$. In the buoyant layer, a flux of volume (Q_P) and buoyancy ($g'_P Q_P$) is provided by the plume and an outlet of flow (Q_T) and buoyancy ($g' Q_T$) occurs through the top opening. In this case, conservation of volume and buoyancy read [17]

$$\begin{cases} A_c \frac{\mathrm{d}}{\mathrm{d}t}(H - h) = Q_P - Q_T, \\ A_c \frac{\mathrm{d}}{\mathrm{d}t}[g'(H - h)] = g'_P Q_P - g' Q_T. \end{cases} \tag{7}$$

The top line in Eqs. (7) models the conservation of volume in the buoyant layer. If the flow rate entering from the plume (Q_P) is different from that leaving from the top opening (Q_T), then a change of the thickness of the buoyant layer ($H-h$) takes place. The bottom line in Eqs. (7) states the conservation of buoyancy in the buoyant layer: a variation of buoyancy ($g'[(H-h]$) occurs if the buoyancy flux provided by the plume ($g'_P Q_P$) is different from that leaving from the top opening ($g' Q_T$).

When $\mathcal{P} < 0$, wind dominates over buoyancy, the flow at the top opening is from outside to inside and reads $Q_T =$

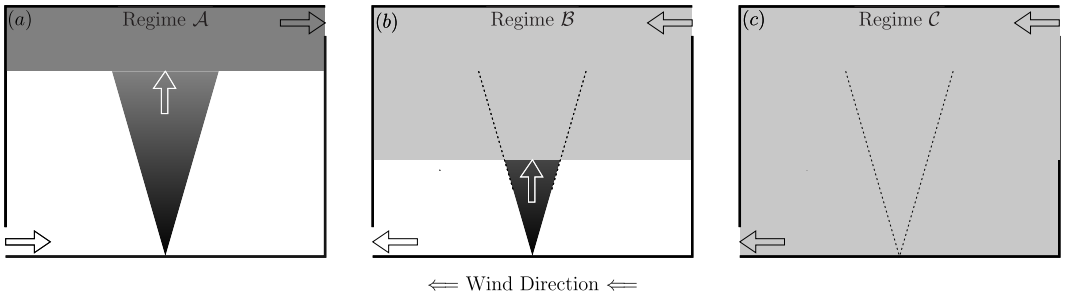

Figure 2: The tree possible regimes that form when the top opening is in the upwind wall and wind contrasts the buoyancy-induced natural ventilation: regime $\mathcal{A}$, "stratified forward flow" (a); regime $\mathcal{B}$, "stratified reverse flow" (b); regime C, "mixed reverse flow" (c). Wind direction is from right to left.

$-A^*\left\{[\Delta p_w/\rho - g'(H-h)]^{1/2}\right\}$. In the buoyant layer, a flux of volume and buoyancy is still provided by the plume. At the top opening, the buoyant layer receive a volume flux Q_T from outside. This income of fresh air does not however imply a buoyancy flux, since fresh air coming from the outside has zero buoyancy (i.e. $g' = 0$). In case that the warm buoyant layer is preserved (regime $\mathcal{B}$), conservation of volume and buoyancy read then [17]

$$\begin{cases} A_c \frac{\mathrm{d}}{\mathrm{d}t}(H-h) = Q_P - Q_T, \\ A_c \frac{\mathrm{d}}{\mathrm{d}t}[g'(H-h)] = g'_P Q_P + g' Q_T = g'_P Q_P + 0 \cdot Q_T = g'_P Q_P. \end{cases} \tag{8}$$

It should be noted that Eqs. (8) describe a progressive increment of the buoyant layer thickness and a progressive decrease of its reduced gravity.

In case of perfectly mixed reverse flows (the warm buoyant layer is not preserved, regime C) , the buoyancy (B_0) is provided by the point source. Such buoyancy instantaneously mixes in the whole inner space of the room. The wind overwhelms buoyancy forces and induces a volume flux entering from the top opening (Q_T). This same flow leaves the room from the bottom opening (Q_B). This wind-induced flow provides the room ventilation, removing buoyancy from the inner space of the room. In this case, the system dynamics are modelled as [17]

$$\begin{cases} h = \mathrm{d}h/\mathrm{d}t = 0, \\ A_c \frac{\mathrm{d}}{\mathrm{d}t}[g'(H-h)] = B_0 - g' Q_B = B_0 - g' Q_T. \end{cases} \tag{9}$$

The first equation states that – in the flow regime C – the stratified flow cannot take place. The second equation in the system (9) states that buoyancy ($g'[H-h]$) variations are driven by the difference between the buoyancy flux provided by the point source B_0 and the buoyancy flux $g'Q_B$ that leaves the room from the bottom opening. In turn, mass conservation implies that $Q_B = Q_T$ and thus $g'Q_B$=$g'Q_T$.

Summing up, equation sets (7)-(9) can be used to model the dynamics of the elevation interface h and of the buoyant layer reduced gravity g', possibly with unsteady strength of buoyancy and unsteady wind velocity.

We stress that these models are based on the assumption that the buoyant layer is fully mixed, a condition that could be verified experimentally in previous works (e.g. [17]). Therefore, the considered equations do not take into account the secondary stratification that might arise within the buoyant layer, associated to a finite value of the density gradient. For this reason, we neglect here the role of an intrinsic frequency of oscillation of the buoyant layer [i.e., the Brunt–Väisälä frequency, 43]. The inclusion of the intrinsic response to oscillations might instead be important in systems where a continuous stratification takes place within the room (e.g., rooms with a distributed buoyancy source) [2].

To make the previous systems of equations dimensionless, it is customary [17, 18] to scale: (i) the lengths, with the room height H; (ii) the reduced gravities, with the reduced gravity of the plume at $z = H$, namely $g'_H = C^{-1}B_0^{2/3}H^{-5/3}$; and (iii) the times, with the so called "filling box time" [17]

$$T_{Bf} = \frac{A_c H}{C B_0^{1/3} H^{5/3}} = \frac{A_c}{C B_0^{1/3} H^{2/3}}. \tag{10}$$

According to Eq. (1), the maximum flow rate of the plume (occurring when the plume reaches the ceiling) is $Q_{P,\max} = CB_0^{2/3}H^{5/3}$. The "filling box time" is thus the time required to fill a box of volume $A_c H$ with a flow rate $Q_{P,\max}$. The application of the aforementioned scaling to Eqs. (7-9) gives the dimensionless model (hat marks dimensionless dynamical variables) [17]

$$-\frac{\mathrm{d}\hat{h}}{\mathrm{d}\hat{t}} = \begin{cases} \hat{h}^{5/3} - |V\hat{P}|^{1/2} & (a) \\ \hat{h}^{5/3} + |V\hat{P}|^{1/2} & (b) \\ 0 & (c) \end{cases} \tag{11}$$

and

$$\frac{\mathrm{d}}{\mathrm{d}\hat{t}}[\hat{g}(1-\hat{h})] = \begin{cases} 1 - |V\hat{P}|^{1/2}\hat{g} & (a) \\ 1 & (b) \\ 1 - |V\hat{P}|^{1/2}\hat{g} & (c) \end{cases}, \tag{12}$$

where

$$V = \left(\frac{A^*}{C^{3/2}H^2}\right)^2, \tag{13}$$

is the so-called "vent parameter". Recalling that: (i) the maximum flow rate through the opening induced by the stack effect is $Q_{T,b,\max} = +A^*[g'H]^{1/2}$ and (ii) the maximum flow rate of the plume (occurring at $z = H$) is $Q_{P,\max} = CB_0^{2/3}H^{5/3}$, it follows that V is the squared ratio $Q_{T,b,\max}/Q_{P,\max}$. Physically, it represents the rate at which warm air is expelled from the room through the top opening, compared to the flow rate of the warm (plume) air source. High values of V denote rooms with wide openings (or a weak buoyancy source), that can easily exchange

buoyant fluid with the external environment. In these conditions, a very warm and thick buoyant layers will hardly form. Conversely, low V values correspond to rooms with small openings (or a strong buoyancy source), that hardly exchange air with the external ambient. In these conditions, it is likely that a warm and thick buoyant layer will occur.

In Eqs. (11-12), the letters $(a)-(c)$ refer to the three regimes $\mathcal{A}-C$ depicted in Fig. 2. In order to determine when a specific regime holds, we evaluate the dimensionless version of Eq. (6), namely

$$\hat{P} = \hat{B} - W, \tag{14}$$

where $\hat{B} = \hat{g}(1-\hat{g})$ represents the (dimensionless) buoyancy of the warm layer and

$$W = \frac{\Delta p/\rho}{g'_H H} \tag{15}$$

is the "wind parameter". It quantifies the strength of the wind, compared to the strength of the stack effect. Since the maximum wind-induced flow rate through the openings is $Q_{T,w,\max} = A^*[\Delta p_w/\rho]^{1/2}$, W is the ratio $Q_{T,w,\max}/Q_{T,b,\max}$. High values of W correspond to a strong wind (or a weak buoyancy source) that can easily cause reverse flow conditions, while low W values denote a weak wind (or a strong buoyancy source) so that reversal of flow conditions is unlikely.

When $P > 0$ the buoyancy prevails over wind and regime $\mathcal{A}$ (stratified forward flow) occurs. When $P < 0$, one of the two reverse-flow regimes can take place. Notably, regime $\mathcal{B}$ occurs when the warm buoyant layer still exists (mathematically, when $\hat{h} > 0$), while regime C takes place when the cold-warm layer interface reaches the room floor (i.e., $\hat{h} = 0$).

In order to focus on the steady state behaviour of a naturally ventilated room, the condition $\mathrm{d}/\mathrm{d}\hat{t} = 0$ is set in the systems (11-12). For regime $\mathcal{A}$, one obtains

$$\hat{g}_0 = \hat{h}_0^{-5/3}, \quad V = \frac{\hat{h}_0^{10/3}}{[\hat{h}_0^{-5/3}(1-\hat{h}_0) - W]}. \tag{16}$$

The solution for these equations exists and is unique for all values of W (see continuous line in Fig. 3). For regime $\mathcal{B}$, no steady state solution exists. Finally, for regime C, the solutions are the roots of the cubic

$$\hat{g}_0^3 - W\hat{g}_0^2 + V^{-1}, \tag{17}$$

where (two) real roots exist only when $W^3V > 27/4$.

The analysis of the stability of these steady solutions (equilibrium configurations) [7], shows that the value $W^3V = 27/4$ is a bifurcation point (see Fig. 3). When $W^3V < 27/4$, only regime $\mathcal{A}$ is possible. When the wind is sufficiently weak, a stratified forward flow (and a buoyant layer) always takes place, independently from the initial conditions. Differently, when $W^3V > 27/4$ two stable configurations are possible. One configuration is regime $\mathcal{A}$. The other configuration is regime C. The corresponding attraction basins are separated by the boundary identified by the second (unstable) solution related to regime C. In this case, the initial conditions determine whether a stratified forward flow (regime $\mathcal{A}$) or a mixed reverse flow (regime C) will develop.

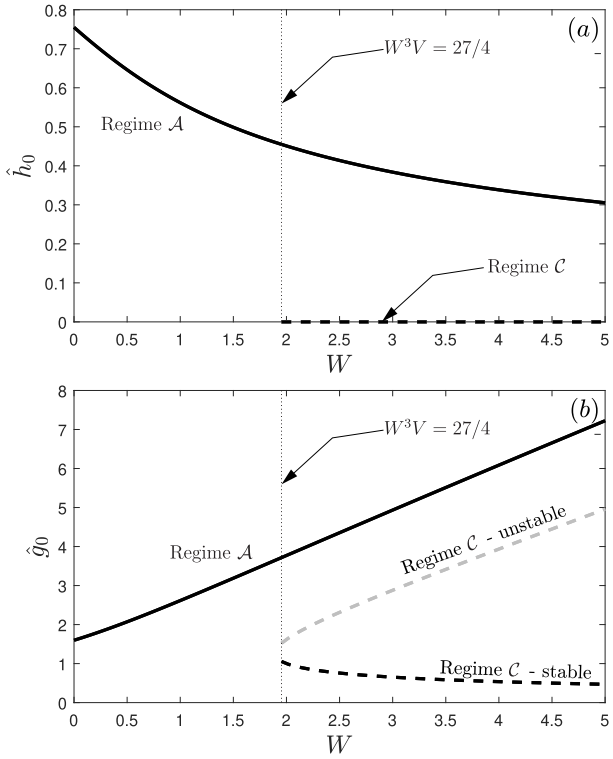

Figure 3: Steady state solutions of the system (11-12). Panel (a) shows $\hat{h}_0$ and panel (b) reports $\hat{g}_0$. The continuous line corresponds to the solution found for regime $\mathcal{A}$; this solution is unique and exists for all values of W. For regime $\mathcal{B}$, no solution exists. The dashed lines refer to the (real) solutions found for regime C. They exist only for $W^3 > 27/4$ and one of them is stable (black line) while the other is unstable (grey line). In panel (a), black and gray dashed lines overlap at $\hat{h}_0 = 0$. The charts refer to $V = 1$.

Table 1: Parameters a and b provided by [44] and corresponding relaxation time τ_{wv} and standard deviation σ_{wv} used in the Ornstein-Uhlenbeck process described by Eq. (20). The values $v_{0,\min}$ and $v_{0,\max}$ delimit the range of mean wind velocity within which the parameters are valid.

a	b	τ_{wv} (s)	σ_{wv} (m/s)	$v_{0,\min}$ (m/s)	$v_{0,\max}$ (m/s)
-0.1619	0.2878	6	0.51	4.00	8.00
-0.0855	0.1700	12	0.41	8.00	9.40
-0.0314	0.2573	32	1.03	9.40	10.20
-0.1049	0.3137	10	0.68	10.20	10.70
-0.0459	0.5118	22	1.69	10.70	11.20
-0.0196	0.2901	51	1.47	11.20	12.00
-0.0683	0.4051	15	1.10	12.00	12.80
-0.0957	0.3008	10	0.69	12.80	25.00

3. Random wind velocity fluctuations

In accordance to the approach usually adopted for studying turbulent flows, the wind velocity can be expressed as

$$v(t) = v_0 + v'(t), \tag{18}$$

where v_0 is the mean velocity and $v'(t)$ is the time-dependent fluctuation around v_0. As customary in wind engineering, we model such fluctuation as an Ornstein-Uhlenbeck stochastic process [45, 46]. It is a stationary colored Gaussian–Markov process with the following characteristics: (i) the probability density function of the realizations $v'(t)$ is a Gaussian distribution with zero mean and standard deviation σ_{wv} (the subscript "wv" stands for "wind velocity"); (ii) the stochastic process is exponentially autocorrelated as $\langle v'(t)v'(t+\tau)\rangle = \sigma_{wv}\exp[-\tau/\tau_{wv}]$, where $\langle\cdot\rangle$ denotes the ensemble average operator and τ_{wv} is the autocorrelation (or relaxation) time; and (iii) the process is stationary, namely σ_{wv} and τ_{wv} do not change over time. In addition, the Ornstein-Uhlenbeck process has a number of attracting analytical properties. Notably, it is possible to change the intensity of fluctuations and their (linear) temporal memory by acting on only two parameters, the standard deviation σ_{wv} and the timescale τ_{wv}. The Ornstein-Uhlenbeck process is adopted to model velocity fluctuations in wind engineering applications for two main reasons. The first reason is the capability of providing wind time series that are realistic (in terms of statistical properties) [34, 32, 47]. The second reason is that it is possible to obtain time-series that span over a wide range of time scales, from seconds up to hours and days [48, 44, 49, 50].

Fluctuation can then be modelled as [51]

$$\mathrm{d}v'(t) = av'(t)\mathrm{d}t + b\mathrm{d}\Omega(t), \tag{19}$$

where $\Omega(t)$ is a standard Brownian motion, $a = -\tau_{wv}^{-1}$, and $b = {c_{wv}}^{1/2}$, where $c_{wv} = 2\sigma_{wv}^2/\tau_{wv}$. The standard Brownian motion (or Wiener Process) $\Omega(t)$ is a martingale (i.e., a continuous sequence of random variables) whose key characteristics are: (i) a mean value equal to zero; (ii) time increments of the sequence normally distributed; and (iii) time increments independent one from the others. An analogy in discrete sequences of numbers is the succession of random extractions from a zero-mean normal distribution. The term b in Eq. (19) is often called "diffusion constant" and indicates how large the deviation from the zero mean is: the greater the wind velocity standard deviation, the greater is the diffusion constant. Finally, the term a is called "speed of the mean reversion" and indicates how fast the variable tends to go back to the mean value. Therefore, the Ornstein-Uhlenbeck process consists of two components. The first component is the stochastic term $b\mathrm{d}\Omega(t)$, which induces random and independent fluctuations. The second component is the deterministic term $av'(t)\mathrm{d}t$ that promotes the damping of such fluctuations and the decay to the mean value (equal to zero). Tab. 3 reports realistic values of the parameters a and b provided by [44] and the corresponding relaxation time τ_{wv} and standard deviation σ_{wv}.

For fixed values of σ_{wv} and τ_{wv}, a realization of the velocity fluctuations time series, $v'(t)$, can be obtained by the so-called "exact update formula" [51] as

$$v'(t+\Delta t) = v'(t)\cdot\zeta + \sigma_{wv}\cdot\sqrt{1-\zeta^2}\cdot n, \tag{20}$$

where n is a random number from a zero-mean unit-variance Gaussian distribution, Δt is the time-step of the process, and $\zeta = \exp[-\Delta t/\tau_{wv}]$. The time series of the stochastic velocity fluctuations $v'(t)$ are here used to generate the time series of the wind parameter $W(t)$. To this aim, Eqs. (2) and (5) are first introduced in Eq. (15). Algebraic manipulations are then performed to isolate $v(t)$ from $W(t)$, obtaining

$$W(t) = \chi v^2(t), \text{ where } \chi = \frac{\left(C_{pu} - C_{pl}\right)}{2C^{-1}\tilde{B}_0^{2/3}\tilde{H}^{-2/3}}. \tag{21}$$

If $v(t) = v_0$ is constant, the wind parameter is also constant and equal to $W(t) = W_0 = \chi v_0^2$. It follows that $\chi = W_0/v_0^2$ and then, in the general case of variable wind velocity,

$$W(t) = \chi v^2(t) = \frac{W_0}{v_0^2}v^2(t) = W_0\left[\frac{v_0 + v'(t)}{v_0}\right]^2 = W_0\left[1 + \frac{v'(t)}{v_0}\right]^2. \tag{22}$$

Eq. (22) highlights the two key ingredients of the time-series $W(t)$. The first ingredient (the base value around which fluctuations take place) is quantified by the mean value of the wind parameter W_0. The second ingredient (the fluctuations) is quantified by the factor $(1 + v'(t)/v_0)^2$. This term shows that the magnitude of wind velocity fluctuations alone is not a key factor: fluctuations magnitude has to be referred to the mean value of the velocity, v_0. It is therefore more convenient to focus on the coefficient of variation of the wind velocity, $C_{V,wv} = \sigma_{wv}/v_0$, rather than on the standard deviation of the wind velocity. It should be finally noted that the temporal scaling can be implemented by dividing t and τ_{wv} by the timescale $\tilde{T}_{Bf}$. In this way, we obtain the dimensionless time $\hat{t}$ and relaxation time $\hat{\tau}_{wv}$.

4. Numerical procedure

In order to investigate the effect of stochastic wind velocity fluctuations on the ventilation dynamics of a room – i.e., on the time-series of the buoyant layer interface elevation $\hat{h}(\hat{t})$ and reduced gravity $\hat{g}(\hat{t})$ – we have performed several numerical simulations, each of them consisting of two steps.

Firstly, we have set the room parameter (i.e., the vent parameter V) and wind characteristics (mean wind W_0 and fluctuation properties $\hat{\tau}_{wv}$ and $C_{V,wv}$), adopting typical literature values and real-world data. Then, the time-series of the wind velocity fluctuations has been simulated according to Eq. (20). We have set $v'(t = 0) = 0$ [a standard choice in the simulation of fluctuations, 36] and $\sigma_{wv} = C_{V,wv} v_0$. The mean velocity was arbitrarily set at the value v_0=1 m/s. Note that this choice does not affect the results because the velocity time series $v(t)$ is normalized with the mean velocity v_0 (see Eq. (22)). Finally, we have set $\Delta t = \tau_{wv}/50$, in order to have a temporal resolution of the simulated time series much finer than the relaxation time of the Ornstein-Uhlenbeck process. For some cases, we have also tested smaller values of Δt, but the results were (statistically) identical. In order to obtain the series of random numbers n_i, $i = 1, ..., N$ (N is the total number of considered time steps of the Ornstein-Uhlenbeck process) required for the generation of the stochastic term of the Ornstein-Uhlenbeck process, a standard Matlab routine (randn) based on the Ziggurat algorithm [52] was used. It should be noted that the same series of random numbers n_i was adopted in each simulation (performed with different values of V, W_0, $\hat{\tau}_{wv}$, and $C_{V,wv}$) in order to keep the results comparable. Different sets of random numbers were later tested, confirming the picture reported here. The duration of the simulations was set equal to $4000\tau_{wv}$, so that $\hat{h}(\hat{t})$ and $\hat{g}(\hat{t})$ could always reach a statistical steady state. It should be finally noted that Eq. (20) is an exact update formula. As a result, no numerical approximations are involved in the evaluation of the velocity fluctuation terms $v'(t+\Delta t)$ starting from $v'(t)$. The corresponding time-series of the wind parameter $W(t)$ was computed according to Eq. (22). Finally, the time series $W(t)$ was mapped from the dimensional time domain t to the dimensionless time domain $\hat{t}$, obtaining the time series of the wind parameter $W(\hat{t})$.

As a second step, Eqs. (11-12) were forced with $W(\hat{t})$. This was done replacing the constant parameter $\hat{P}$ with the time-dependent parameter (see Eq. (14)) $\hat{P}(\hat{t}) = \hat{B} - W(\hat{t})$. To facilitate the solution of Eqs. (11-12), the term $\hat{g}(1-\hat{h})$ was replaced by the new variable $G = \hat{g}(1-\hat{h})$, so that $\hat{g} = G/(1-\hat{h})$. Eqs. (11-12) could be then written as

$$-\frac{\mathrm{d}\hat{h}}{\mathrm{d}\hat{t}} = \begin{cases} \hat{h}^{5/3} - |V\hat{P}(\hat{t})|^{1/2} & (a) \\ \hat{h}^{5/3} + |V\hat{P}(\hat{t})|^{1/2} & (b) \\ 0 & (c) \end{cases} \tag{23}$$

and

$$\frac{\mathrm{d}G}{\mathrm{d}\hat{t}} = \begin{cases} 1 - |V\hat{P}(\hat{t})|^{1/2} G(1-\hat{h})^{-1} & (a) \\ 1 & (b) \\ 1 - |V\hat{P}(\hat{t})|^{1/2} G(1-\hat{h})^{-1} & (c) \end{cases}, \tag{24}$$

In a more compact notation, the equations read

$$\frac{\mathrm{d}\mathbf{X}}{\mathrm{d}\hat{t}} = \begin{cases} f_1(X_1, X_2, V, \hat{P}(\hat{t})) \\ f_2(X_1, X_2, V, \hat{P}(\hat{t})) \end{cases}, \tag{25}$$

where $\mathbf{X} = \{X_1, X_2\} = \{\hat{h}, G\}$, f_1 is one of the functions reported in Eqs. (23), and f_2 is one of the functions reported in Eqs. (24). For each time step of the simulation, the selection of the actual functions f_1 and f_2 is based on the value taken by the parameter $\hat{P}(\hat{t})$ and by the value of $\hat{h} = X_1$ at the beginning of the time step. In particular, Eqs. (23a) and (24a) are selected when $\hat{P}(\hat{t}) > 0$; Eqs. (23b) and (24b) are considered when $\hat{P}(\hat{t}) < 0$ and $\hat{h} > 0$; Eqs. (23c) and (24c) are selected when $\hat{P}(\hat{t}) < 0$ and $\hat{h} = 0$.

The initial conditions are $\hat{h}(\hat{t} = 0)$=$\hat{h}_0$ and $G_0 = G(\hat{t} = 0)$=$\hat{g}_0(1-\hat{h}_0)$. The values $\hat{h}_0$ and $\hat{g}_0$ correspond to the equilibrium configuration obtained from Eq. (16) (regime $\mathcal{A}$) or Eq. (17) (regime C) with $W = W_0$.

The numerical integration of Eq. (25) implies no particular difficulties, and can be easily performed using commercially available solvers for ordinary differential equations. In particular, the formulation of Eq. (25) can be given as input without modifications to the built-in Matlab routine "ode45" (adopted in our calculations). This routine implements an explicit Runge-Kutta method, using the Dormand-Prince pair approach [53]. We have tested the aforementioned numerical procedure by comparing the results obtained with our scripts with published results [17] in the case of deterministic conditions, without observing any discrepancy. Finally, the time series $\hat{g}(\hat{t})$ could be obtained from the time series $G(\hat{t})$ and $\hat{h}(\hat{t})$ with the simple algebraic relation $\hat{g}(\hat{t})$=$G(\hat{t})/\hat{h}(\hat{t})$.

5. Results

5.1. Zero-mean wind fluctuations alter the average elevation of the cold-warm air interface

To investigate the influence of the stochastic forcing on the system dynamics, we begin by examining few emblematic examples. In order to enlighten the main peculiarities of the stochastic forcing case – compared to the constant wind case – we evaluated the metrics $\eta(\hat{t}) = \hat{h}(\hat{t})/\hat{h}_0$ and $\gamma(t) = \hat{g}(t)/\hat{g}_0$. $\hat{h}_0$ and $\hat{g}_0$ refer to regime $\mathcal{A}$, so that $\eta(\hat{t})$ and $\gamma(\hat{t})$ quantify the deviation of the system forced by a stochastically varying wind from the same system with a constant wind and where a stratified forward flow (regime $\mathcal{A}$) takes place. The values $\eta = \gamma = 1$ indicate that no modification occurs, whereas $\eta < 1$ and $\gamma < 1$ indicate that the buoyant layer interface and the reduced gravity are lower than those in the constant wind case. Note that the values $\eta > 1$ and $\gamma > 1$ never occurred in the simulations.

Fig. 4 shows a few time series of η and γ evaluated for $V = 1$, $C_{V,wv} = 0.1$, $\tau_{wv} = 0.005$, and mean wind parameters $W_0 = 1$, 1.5, 2 (a systematic analysis of of the model response in the parameter space will be provided in Secs. 5.2 and 5.3).

We focus first on the time series obtained adopting the initial conditions $\hat{h}(\hat{t} = 0) = \hat{h}_0$ and $\hat{g}(\hat{t} = 0) = \hat{g}_0$ evaluated from Eq. (16). Namely, at $\hat{t} = 0$, the system is in an equilibrium configuration with a stratified forward flow (regime $\mathcal{A}$). The corresponding curves $\eta(\hat{t})$ and $\gamma(\hat{t})$ are plotted in Fig. 4 with

thick continuous lines. For all the three considered cases (W_0 = 1, 1.5, 2), we observe a similar temporal pattern: (i) at $\hat{t} = 0$ the system is at the equilibrium conditions found at the steady state, namely $\eta(\hat{t})=\gamma(\hat{t})=1$; (ii) over the time interval $0 < \hat{t} \lesssim 2$, η and γ reduce significantly; and (iii) for $\hat{t} \gtrsim 2$ the system recovers a new condition of dynamic equilibrium around which $\eta(\hat{t})$ and $\gamma(\hat{t})$ oscillate, in response to the persistent random forcing. The larger is W_0, the larger are the deviations of η and γ from unity and the larger are the amplitude of the fluctuations of η (during the dynamic equilibrium phase). Fluctuations of γ are instead less sensitive to variations of W_0.

For the case $W_0 = 2$, which is beyond the bifurcation threshold $W_0^3/V > 27/4$, we also tested the two initial conditions $\hat{h}(\hat{t} = 0) = \hat{h}_0$ and $\hat{g}(\hat{t} = 0) = \hat{g}_0$ evaluated from Eq. (17) (i.e., at $\hat{t} = 0$, the system is in an equilibrium configuration characterized by the mixed reverse flow of regime C). The two initial conditions (equilibrium configurations) have the same initial value $\hat{h}_0 = 0$, but different values of $\hat{g}_0$. The case corresponding to the unstable equilibrium configuration (red dashed line in Fig. 4) exhibits a transient phase which drives the system to the same conditions of dynamic equilibrium attained when the initial condition is evaluated from Eq. (16) (stratified forward flow, see the red continuous line in Fig. 4). The case with an initial condition equal to the stable equilibrium configuration (red dotted line in Fig. 4) is almost insensitive to wind fluctuations: $\eta(\hat{t})$ remains constant at the value $\eta(\hat{t}) = 0$ (mixed reverse flow) and $\gamma(\hat{t})$ exhibits small fluctuations.

The emblematic examples previously discussed highlight a major feature. A stochastic perturbation (with zero mean) added to a constant wind does not just induce fluctuations with zero mean around the system steady-configuration of equilibrium attained with constant wind. As a matter of facts, the stochastic noise alters the averaged behaviour of the system (compared to the system constant-wind-configuration), inducing a reduction in the interface elevation and reduced gravity of the buoyant layer.

In order to explain the physical reasons of this peculiar behaviour, we consider the response of a ventilated room in which the wind parameter $W(t)$ evolves as a periodic square wave (see top panel in Fig. 5), switching above and below the mean value W_0 of the same amount ΔW and keeping the values $W_0 + \Delta W$ or $W_0 - \Delta W$ for the same time interval.

We assume that the system is initially in an equilibrium configuration of stratified forward flow (regime $\mathcal{A}$) and submitted to a constant wind (time interval TI1 in Fig. 5). The dimensionless buoyancy $\hat{B}$ is larger than the wind parameter W (see Eq. 14), wind forces are overcome by the internal buoyancy, and the flow through the top opening is $Q_T > 0$ (i.e., flow of warm air and buoyancy out of the room, see Fig. 5*a*).

The condition of equilibrium (given by Eq. 16) implies that $\hat{h}_0^{10/3} = V[\hat{g}_0(1-\hat{h}_0)-W] = V[\hat{B}_0-W]$. If equilibrium conditions are broken (because of changes in W), the system tends toward a new equilibrium. In the case of an increment of W, wind contrasts more the ejection of warm air from the top opening and the new equilibrium configuration is characterized by lower values of $\hat{h}_0$ and $\hat{g}_0$. Differently, in the case of a reduction of W, the ejection of warm air from the top opening is less contrasted by the wind, and the new equilibrium configuration exhibits higher values of $\hat{h}_0$ and $\hat{g}_0$.

Bearing in mind these possible system responses, we observe that an increment of the wind parameter occurs at the beginning of TI2, changing $W(t)$ instantaneously W_0 to $W_0 + \Delta W$ (see top panel in Fig. 5). An imbalance between wind and buoyancy arises, and therefore the system tends toward a new configuration of equilibrium characterized by an increased thickness of the warm layer ($H - h$). As a result, a strong reduction of h takes place (see the arrow "A" in Fig. 5*b*). In this case the wind parameter W is larger than the dimensionless buoyancy $\hat{B}$ and, according to Eq. (14), cold air enters from the top opening ($Q_T < 0$, see Fig. 5*b*), reducing g'. Summing up, at the end of TI2, the increment of the wind strength has caused a severe reduction of h and g', compared to the initial equilibrium conditions (see Fig. 5*b*).

We now examine the response of the system to the reduction of the wind parameter (from $W_0 + \Delta W$ to $W_0 - \Delta W$) that occurs during TI3 (see top panel in Fig. 5). The imbalance between wind and buoyancy is now in favor of the latter. The new equilibrium configuration towards which the system tends is characterized by a reduced thickness of the warm layer. As a result, a modest increment of h takes place (see the arrow "B" in Fig. 5*c*). A stratified forward flow regime holds, warm air and buoyancy leave the room from the top opening ($Q_T > 0$, see Fig. 5*c*), and g' increases. Differently to what can be observed in TI2 (when the buoyant layer thickness underwent a strong increment), during TI3 the reduction of the buoyant layer thickness is very limited. The reason behind this behaviour is that during TI2 the cold air entering from the top opening reduced g' to a great extent. By contrast, the warm air provided by the plume to the buoyant layer during TI3 is poorly effective in increasing g'. This difference of behaviour during TI2 and TI3 implies that the increase in thickness of the warm layer during TI2 is not fully recovered during TI3. Summing up, at the end of TI3, g' has undergone a modest increment and also h has increased, but they have not reached the initial equilibrium conditions (see the arrow "B" in Fig. 5*c*). It follows that the interval pair TI2-TI3 leads to a decreasing trend of h and g'. This interplay between increasing/decreasing phases of W is the key to understand the decreasing trend of η and γ observed in Fig. 4, for $\hat{t} \lesssim 2$.

We now explain how a ventilated system finally reaches the dynamic equilibrium regime observed after the initial transient (i.e., for $\hat{t} \gtrsim 2$ in Fig. 4). To do this, we repeat the analysis performed so far for TI1 ($W(t) = W_0$), TI2 ($W(t)$ increases to $W_0 + \Delta W$) and TI3 ($W(t)$ reduces to $W_0 - \Delta W$), but focusing on the dynamic equilibrium phase (TI4-TI6 in Fig. 5*d*).

TI4 represents a condition of dynamic equilibrium, and its main characteristics are: (i) the reduced gravity g' of the buoyant layer is significantly lower than g' at the top of the plume (see the different tones of gray in Fig. 5*d*); and (ii) the interface elevation h of the buoyant layer is significantly lower than the interface elevation attained during TI1 (see in Fig. 5*d* the dotted line representing the equilibrium configuration with constant wind).

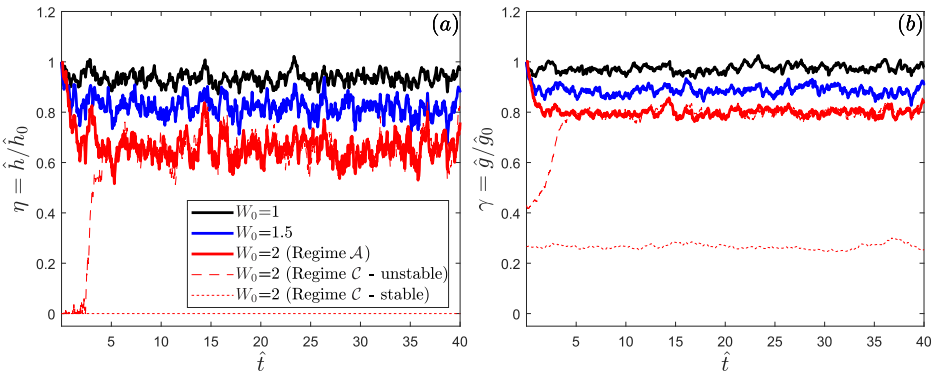

Figure 4: Time series of η (a) and γ (b) for different values of the mean wind parameter (W_0 = 1, 1.5, 2). The other parameters are V = 1, $C_{V,wv}$ = 0.1 and τ_{wv} = 0.005. Thick continuous lines refer to initial conditions equal to the equilibrium configuration of regime $\mathcal{A}$ and evaluated from Eq. (16). Dashed and dotted lines refer to initial conditions equal to the stable and unstable equilibrium configuration of regime $\mathcal{C}$, respectively, and evaluated from Eq. (17).

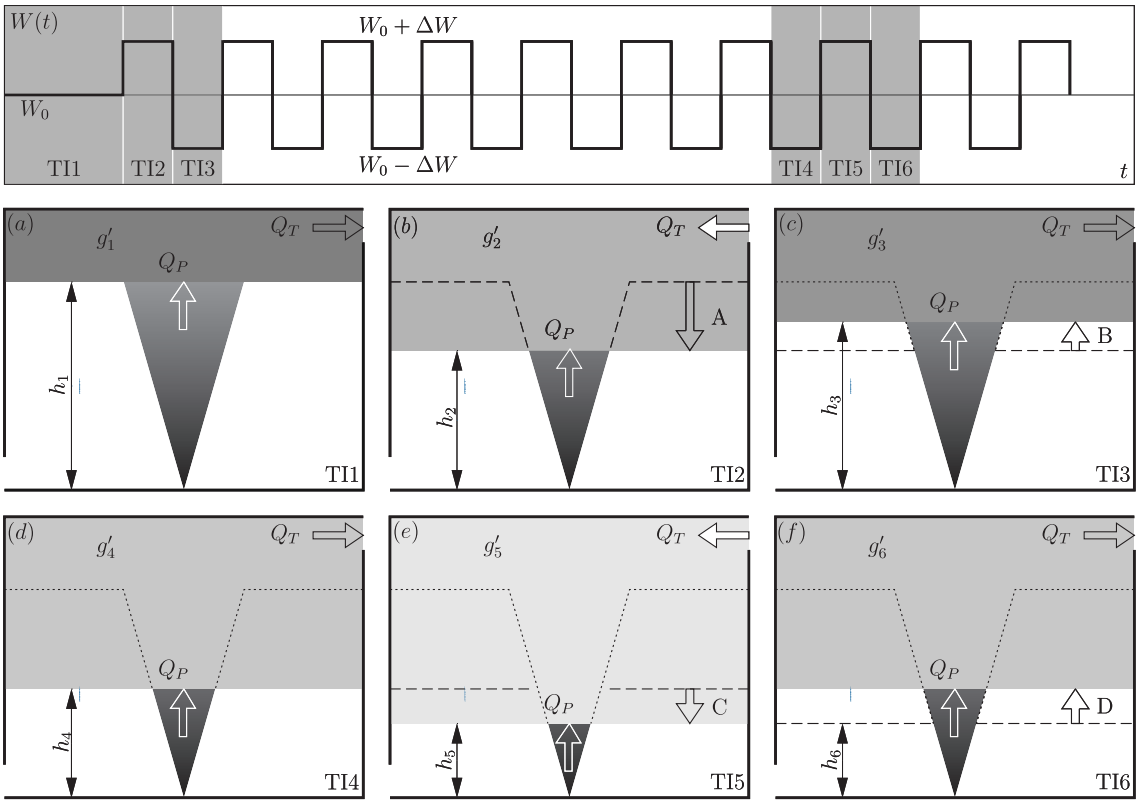

Figure 5: Schematic explanation of the physical mechanism underpinning the alteration of the average elevation of the cold-warm air interface. For simplicity, $W(t)$ is supposed to evolve as a square wave, as depicted in the top panel. Each plot represents a time interval (see the indication "TI" in the lower right corner and the corresponding position in the top panel). In each plot, the shaded zone denotes the system at the end of the time interval, dashed lines denote the system at the begin of the time interval, and dotted lines denote the system at equilibrium (i.e., when $W(t) = W_0$). Vertical arrows indicate the direction of displacement of the buoyant layer interface during the considered time interval. Different grey intensities of the plume and of the buoyant layer denote different values of reduced gravity: white is the lowest (equal to zero, outside), black is the highest (at the point source of buoyancy); intermediate tones of gray stand for intermediate values of reduced gravity.

TI5 and TI6 exhibit dynamics very similar to TI2 and TI3. During TI5 (W rises from $W_0 - \Delta W$ to $W_0 + \Delta W$): (i) the thickness of the warm layer ($H - h$) increases (see the arrow "C" in Fig. 5*e*); (ii) cold air enters from the top opening (see Fig. 5*e*); and (iii) the the reduced gravity g' reduces. During TI6 (W reduces from $W_0 + \Delta W$ to $W_0 - \Delta W$): (i) the buoyancy and the thickness of the warm layer reduce (see the arrow "D" in Fig. 5*f*); (ii) warm air and buoyancy leave the room from the top opening (see Fig. 5*f*); and (iii) g' increases.

We can however observe a key difference between the dynamics occurring during TI2 and TI3 and those occurring during TI5 and TI6. The reduction of g' during TI5 is much lower than that occurring during TI2, even though the system undergoes the same wind alteration that lasts for the same duration. The reason underpinning this behaviour lies on the reduced gravity difference $\Delta g'_a$ between the warm buoyant layer and the cold ambient air. During TI2, $\Delta g'_a$ was high. This implies that the inflow of a volume V_a of cold air reduced to a significant extent g' in the buoyant layer. During TI5, $\Delta g'_a$ is much lower than during TI2. As a result, the inflow of the same volume V_a of cold air reduces to a lower extent g'.

Similarly, the increment of g' occurring during TI6 is much higher than its increment during TI3. Again, the motivation of this behaviour is related to the reduced gravity difference $\Delta g'_P$ between the buoyant layer and the plume. During TI3, $\Delta g'_P$ was low, and the inflow of a volume V_P of warm air from the plume altered to a modest extent the reduced gravity. During TI6, $\Delta g'_P$ is much higher than $\Delta g'_P$ attained during TI3. As a result, the inflow of the same volume V_P of warm air increases to a much higher extent the reduced gravity g' in the buoyant layer.

Summing up: (i) at the end of TI5, h and g' decreased compared to their value at the beginning of the time interval (see Fig. 5*e*). Notably, the reduction of g' during TI5 is lower than that attained during TI2 (compare arrows "A" and "C" in Figs. 5*b* and 5*e*); and (ii) at the end of TI6, both g' and h increased, reaching the conditions met at the end of TI4 (see Fig. 5*f*). Importantly, the increment of g' during TI6 is higher than that attained during TI3 (compare arrows "B" and "D" in Figs. 5*c* and 5*f*). This means that the system has finally reached a dynamical equilibrium, with h and g' oscillating around constant average values.

5.2. Effect of noise parameters

In order to analyse the role of the wind forcing (W_0, $C_{V,wv}$ and $\hat{\tau}_{wv}$) and building (V) characteristics, we define the average interface elevation η_{eq} and reduced gravity γ_{eq} attained during the dynamical equilibrium phase as

$$\eta_{eq} = \frac{1}{T_{fin} - T_{eq}} \int_{T_{eq}}^{T_{fin}} \eta(t)\mathrm{d}t \qquad \gamma_{eq} = \frac{1}{T_{fin} - T_{eq}} \int_{T_{eq}}^{T_{fin}} \gamma(t)\mathrm{d}t, \tag{26}$$

where T_{eq} and T_{fin} delimit the temporal range of the dynamical equilibrium phase.

Figs. 6$a - b$ illustrate the influence of the coefficient of variation $C_{V,wv}$ and of the correlation time $\hat{\tau}_{wv}$ on η_{eq} and γ_{eq} The coefficient of variation $C_{V,wv}$ spans from 0.05 to 0.15, coherently with real data reported in Tab. 3 that show coefficient of variation in the range [0.0275, 0.158]. We did not considered values of $C_{V,wv}$ below 0.05 because preliminary tests indicated that the noise-induced effect was negligible. The dimensionless correlation time $\hat{\tau}_{wv}$ falls in the range [0.01, 0.10] according to real data (reported in Tab. 3) that show correlation times in the range [6, 51] s. These dimensional values of correlation time are to be made dimensionless with the filling box time T_{Bf}. For such parameter, typical values are of the order of 500 s (see Sect. 6). Figure 6 shows four key features. Firstly, equilibrium configurations obtained with a constant $W(t) = W_0$ and (dynamic) equilibrium configurations obtained with a fluctuating $W(t)$ can be very different. These differences are relevant in a wide portion of the parameter space $\{C_{V,wv}, \hat{\tau}_{wv}\}$. The minimum value of γ_{eq} is 0.65 while the minimum value of η_{eq} is 0.35. This means that, compared to the case with a constant wind, wind fluctuations can reduce by 1/3 the buoyant layer interface height and by 2/3 the reduced gravity.

Secondly, the role of the coefficient of variation of the wind velocity, $C_{V,wv}$, is very high, both on γ_{eq} and η_{eq}. For low values of $C_{V,wv}$, γ_{eq} and η_{eq} approach unity, whereas they reduce significantly for higher values.

Thirdly, the role of the correlation time of the wind velocity, $\hat{\tau}_{wv}$, is generally low; it is more impacting on η_{eq} rather than on γ_{eq} and is more relevant when higher values of $C_{V,wv}$ are considered. It is interesting to discuss the different effect of $C_{V,wv}$ and $\hat{\tau}_{wv}$ in causing deviations of η_{equ} and γ_{equ} from unity. High values of $C_{V,wv}$ are related to a high deviation of $W(t)$ from W_0 (i.e., high values of ΔW as defined in the previous section). High values of $\hat{\tau}_{wv}$ are instead related to a long duration of the deviation of $W(t)$ from W_0 (i.e., long time intervals as defined in the previous section). We have previously shown that $C_{V,wv}$ is more impacting than $\hat{\tau}_{wv}$. This suggest that the duration of the time interval during which $W(t)$ deviates from W_0 is less impacting than the magnitude of the deviation ΔW=$W(t) - W_0$.

Fourthly, the influence of the wind parameter can be very relevant. Systems characterised by a low intensity of mean wind are hardly affected by its fluctuations. Indeed, the black curves in Fig. 6 (corresponding to $W_0 = 1$) show that η_{eq} and γ_{eq} are very close to unity. By contrast, red curves (that refer to a stronger wind, i.e. $W_0 = 2$) exhibit larger deviations from unity.

5.3. Influence of the ventilation parameter and mean wind intensity

Fig. 7 shows the influence of the ventilation parameter V and wind parameter W_0 on γ_{eq} (Fig. 7*a* with corresponding zoom in Fig. 7*c*) and η_{eq} (Figs. 7$b - d$). For each pair $\{V, W_0\}$, we simulated all combinations of $C_{V,wv}$×$\hat{\tau}_{wv}$ in the ranges [0.05, 0.10, 0.15]×[0.01, 0.05, 0.1]. Among the nine values of γ_{eq} and η_{eq} obtained for these simulations, we report in the maps the minimum values obtained, which always occurred for $C_{V,wv}$=0.15 and $\hat{\tau}_{wv}$=0.1.

Inspection of Fig. 7 reveals the existence of three zones. The first zone (denoted in yellow) is characterized by values $\eta_{eq} \sim 1$ and $\gamma_{eq} \sim 1$ and corresponds to low values of V and/or low values of W_0. A low value of W_0 means that wind is very weak, whereas a low value of V (see Eq. 13) entails buoyancy-dominated dynamics, either because the buoyancy source is

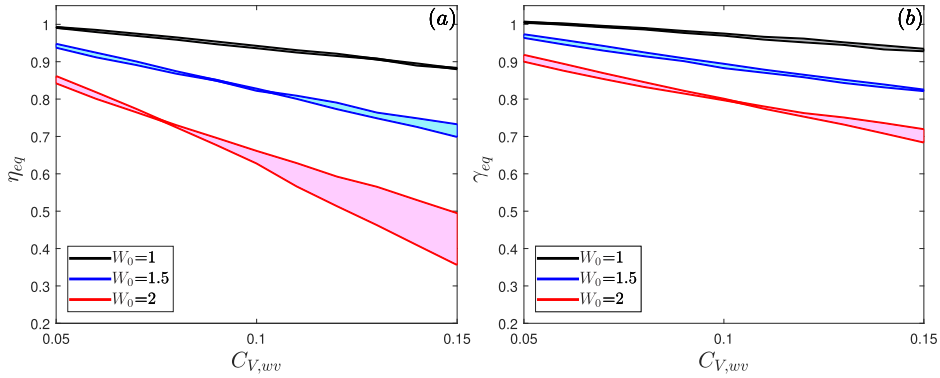

Figure 6: Effect of the noise parameters $C_{V,wv}$ on the average interface elevation η_{eq} (a) and average reduced gravity γ_{eq} (b). The dimensionless correlation time $\hat{\tau}_{wv}$ was varied from 0.05 (highest curves for a given W) to 0.15 (lower curve). Shaded areas refer to values of $\hat{\tau}_{wv}$ between these two boundaries. The venting parameter is $V = 1$.

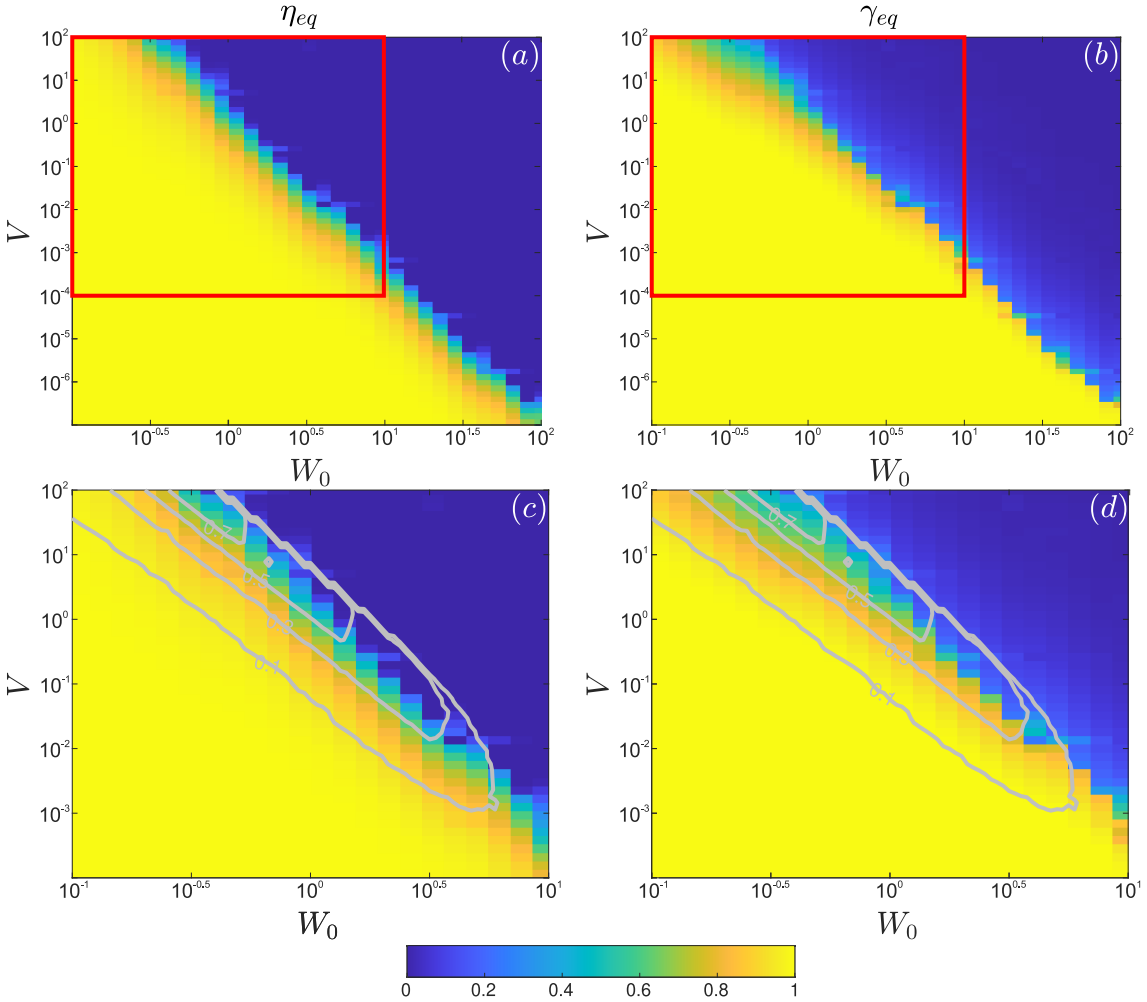

Figure 7: Effect of the venting parameter V and mean wind W_0 on η_{eq} (a) and γ_{eq} (b). The figure reports the largest attained deviations of η_{eq} and γ_{eq} from unity. $C_{V,wv}$ and $\hat{\tau}_{wv}$ spanned ranges [0.05-0.15] and [0.01-0.1], respectively. Red rectangles delimit the zoomed view reported in panels (c) and (d). The gray curves are iso-lines of the "overshoot" ($\hat{h}_0 - \hat{h}_{\min}$]) as defined in [17].

very strong or because openings are very small. In both cases, the effect of wind (and thus wind fluctuations) is almost negligible.

This picture is completely reversed in the second zone (denoted in blue in Fig. 7), corresponding to high values of both V and W_0, where $\eta_{eq} \sim 0$ and $\gamma_{eq} \sim 0$, witnessing the relevant influence of wind on the system dynamics. In this region of the space parameters, the "mixed reverse flow" (regime C) usually occurs. As shown in Sec. 5.1 (see also the dotted red curves in Fig. 4), wind fluctuations are not very relevant and the buoyant layer does not exist.

The third, intermediate zone (colors from yellow to blue), is characterized by values of η_{eq} and γ_{eq} in the interval [0,1]. In this zone, a balance between wind-induced and buoyancy-induced forces exists, providing the ideal conditions to trigger the rich dynamical behaviour depicted in the previous sections. Note that significant deviation of η_{eq} and γ_{eq} from unity are possible in a wide range of the V and W_0 parameters. Notably, η_{eq} exhibits deviations from unity for all the considered values of V, spanning in the range $[10^{-7}, 10^{2}]$). Beside, γ_{eq} shows deviations from unity in a narrower range of V (compared to η_{eq}), i.e., $V \gtrsim 10^{-4}$.

To conclude this section, we discuss our results in the light of the overshoot analysis performed by [17]. They studied the (deterministic) transient dynamics of the interface elevation $\hat{h}(t)$ in regime $\mathcal{A}$, from the condition $\hat{h}(\hat{t} = 0) = 1$ (i.e., a buoyant layer confined at the ceiling of the room) to the equilibrium condition $\hat{h}(\hat{t} \to \infty) = \hat{h}_0$. [17] found that the path leading to the equilibrium exhibits – in some cases – an overshoot in the initial stages (during which $\hat{h}(t)$ suddenly decreases, in some cases reaching a minimum value $\hat{h}_{\min}$, so that $\hat{h}_{\min} < \hat{h}_0$), and rebounds next, finally attaining the equilibrium value $\hat{h}_0$. As done by [17] in their work (see Figure 4 of their paper), we map in Fig. 7 iso-lines of the difference $\hat{h}_0 - \hat{h}_{\min}$ (defined by [17] as the "overshoot size"). Interestingly, the portion of space parameter $\{V, W_0\}$ where we observe the highest deviation from unity of η_{eq} is the same in which the most relevant overshoots occur. This region of the parameter space appears to be the epicenter of a rich interplay of competing mechanisms, affecting the subtle balance between wind-induced and buoyancy-induced effects. When this balance is perturbed – by wind fluctuations in our case, or by an initial offset from equilibrium condition in [17] – the system is prone to amplify disturbances. When the system is forced by a continuous stochastic wind, the configuration of dynamical equilibrium attained can be very different from that attained when a constant wind is present.

6. A real case study

In order to show the effect of wind fluctuations on a real case study, we consider a conference room similar to the room analysed by [4]. The cross-sectional area is A_c=50 m^2, the height is H = 4 m, and two openings are cut in the upwind and downwind face, with effective flow area equal to A^*= 0.63 m^2. Inside the room, a thermal load with power E =2000 W (e.g., 13 people sitting around a conference table) exists. The thermal load generates the buoyancy $B_0 = g\beta E/(\rho c_p) = 5.5 \cdot 10^{-2}$ m^{4}s^{-3}, where $\beta = 3.48 \cdot 10^{-3}$ K^{-1} and $c_p = 1012$ J kg^{-1} K^{-1} are the coefficient of thermal expansion and the specific heat capacity of air, respectively. At the ceiling, the reduced gravity is (computed by Eq. 2) g'_H =0.12 m/s^2. Wind blows at the mean velocity v_0=1.40 m/s . For the sake of simplicity, we consider $\left(C_{pu} - C_{pl}\right) = 1$ [40]. Under these assumptions, the wind induces (according to Eq. 5) a mean pressure difference $\Delta p_{w,0}$ = 1.22 Pa.

Given these parameters, the vent parameter and the mean wind parameter are (Eqs. 13 and 15) V = 1.00 and W_0 = 2.00 (a pair considered in Figs. 4 and 6). Moreover, the box filling time (Eq. (10)) is T_{Bf}= 452 s.

According to Eq. (16), the equilibrium configuration of regime $\mathcal{A}$ (forward stratified flow) is $\hat{h}_0$=0.45 and $\hat{g}_0$=3.77.

We first neglect wind fluctuations, with a room ventilation affected by a constant wind v_0, which implies a reduced gravity within the buoyant layer g' = 0.45 m/s^2 and an elevation of its interface h = 1.80 m. It follows that people (whose height is usually less than 1.80 m) breath below the warm buoyant layer. Moreover, the flow rate of fresh air that enters the room from the bottom opening (in equilibrium conditions $Q_P = Q_T = Q_B$), computed by means of Eq. (1), is equal to 0.12 m^3/s, i.e. 2.1 air changes per hour.

We now consider the case of a fluctuating wind. Assuming a (reasonable) coefficient of variation $C_{V,wv}$ = 0.10, the corresponding correction factors are $\eta_{eq} \sim 0.6$ and $\gamma_{eq} \sim 0.8$ (see Fig. 6). Accordingly, the reduced gravity within the buoyant layer is $g' \simeq 0.36$ m/s^2, the elevation of the interface is h = 1.10 m, the air exchange flow is Q_P = 0.05 m^3/s, and only 0.9 air changes per hour occur. The ventilation conditions have therefore changed dramatically, for the worse, compared to the case of a constant wind. People in the room breath now well above the warm buoyant layer, which implies conditions that are (i) less comfortable, due to the high temperature and humidity and (ii) potentially dangerous, as human exhalations mix and can be inhaled. This simple example evidences the crucial impact of wind fluctuations on the natural ventilation of a room.

7. Conclusions

We studied the ventilation dynamics of a room characterized by the presence of a point buoyancy source and submitted to the action of an unsteady opposing wind, which was modelled here by adding a random forcing to the governing equations. Our focus was on the impact of wind fluctuations on the elevation of the interface of the buoyant layer, that accumulates at the ceiling of the room, and on its reduced gravity. Our results show that the average elevation attained under the effect of a fluctuating wind can be much different from what observed when a constant wind is considered. Typically, the interface elevation of the buoyant layer tends to decrease (up to a third), as does its reduced gravity.

This peculiar and unexpected behaviour was thoroughly investigated. A physically-based explanation was given and a parametric study was performed, focusing on the role of (i) the intensity and time correlation of wind fluctuations and (ii) the

vent and wind parameters. Most of these parameters have a relevant effect in the dynamics that drive the reduction of the buoyant layer interface elevation and reduced gravity (compared to the case of constant wind). The only parameter that has a marginal influence on the system dynamics is the time-correlation of the wind velocity fluctuations (at least in the range of realistic timescales here considered). Finally, we analyzed an example of real naturally-ventilated room to show that a randomly fluctuating wind can lead to a worsening of the ventilation performances, which implies a considerable reduction of the comfort and safety of naturally ventilated enclosed spaces.

It is worth to highlight the interest of the results here reported in the context of reliable and sound design of ventilation systems based on stack effect. We demonstrated that realistic fluctuations of the wind velocity can have a remarkable impact on the dynamics of the buoyant layer interface. In particular, we showed that considering the mean wind velocity can lead to severe errors in the assessment of the ventilation performance of a room. We also evaluated – qualitatively – the amount of these errors and, more importantly, we determined the regions of the parameter space within which wind fluctuations play a crucial role. In order to deal with the uncertainties resulting from wind fluctuations, ventilation engineers can: (i) design ventilation system so that the vent parameter V and the wind parameter W do not fall in the regions prone to noise-induced phenomena or; (ii) compute the interface elevation by considering the mean wind velocity and then applying correction coefficients (e.g., those in Fig. 6) to account for effects due to wind velocity fluctuations.

It should be finally noted that the scientific community is increasingly highlighting the role of random components in inducing structural changes in the behaviour of a dynamic system (the so-called 'noise-induced phenomena'). This study shows that natural ventilation also exhibits this fascinating feature, which should be considered for effective design, given the ubiquity of wind fluctuations.

Declaration of competing interest

The authors declare that they have no known competing financial interests or personal relationships that could have appeared to influence the work reported in this paper.

Acknowledgements

This research did not receive any specific grant from funding agencies in the public, commercial, or not-for-profit sectors.

Data availability

No data were used in this work.

References

[1] P. Linden, G. Lane-Serff, D. Smeed, Emptying filling boxes: The fluid mechanics of natural ventilation, J. Fluid Mech. 212 (1990) 309 – 335. doi:10.1017/S0022112090001987.

[2] P. Linden, The fluid mechanics of natural ventilation, Ann. Rev. Fluid Mech. 31 (1999) 201 – 238. doi:10.1146/annurev.fluid.31.1.201.

[3] G. Hunt, P. Linden, The fluid mechanics of natural ventilation - displacement ventilation by buoyancy-driven flows assisted by wind, Build. Environ. 34 (6) (1999) 707 – 720. doi:10.1016/S0360-1323(98)00053-5.

[4] B. Lishman, A. W. Woods, The control of naturally ventilated buildings subject to wind and buoyancy, J. Fluid Mech. 557 (2006) 451 – 471. doi:10.1017/S0022112006009931.

[5] J. Yuan, L. R. Glicksman, Transitions between the multiple steady states in a natural ventilation system with combined buoyancy and wind driven flows, Build. Environ. 42 (10) (2007) 3500 – 3516. doi:10.1016/j.buildenv.2006.10.045.

[6] G. Hunt, P. Linden, Steady-state flows in an enclosure ventilated by bouyancy forces assisted by wind, J. Fluid Mech. 426 (2001) 355 – 386. doi:10.1017/S0022112000002470.

[7] G. Hunt, P. Linden, Displacement and mixing ventilation driven by opposing wind and buoyancy, J. Fluid Mech. 527 (2005) 27–55. doi:10.1017/S0022112004002575.

[8] H. Montazeri, B. Blocken, Cfd simulation of wind-induced pressure coefficients on buildings with and without balconies: Validation and sensitivity analysis, Build. Environ. 60 (2013) 137 – 149. doi:10.1016/j.buildenv.2012.11.012.

[9] J. M. Holford, G. R. Hunt, Fundamental atrium design for natural ventilation, Build. Environ. 38 (3) (2003) 409 – 426. doi:10.1016/S0360-1323(02)00019-7.

[10] R. W. Mott, A. W. Woods, Natural ventilation driven by periodic gusting of wind, J. Fluid Mech. 679 (2011) 58 – 76. doi:10.1017/jfm.2011.122.

[11] X. Yang, G. Wang, K. Zhong, Y. Kang, Transient pollutant flushing of buoyancy-driven natural ventilation, Build. Simul. 5 (2) (2012) 147 – 155. doi:10.1007/s12273-012-0077-4.

[12] R. K. Bhagat, M. Davies Wykes, S. B. Dalziel, P. Linden, Effects of ventilation on the indoor spread of covid-19, J. Fluid Mech. 903. doi:10.1017/jfm.2020.720.

[13] R. K. Bhagat, P. Linden, Displacement ventilation: A viable ventilation strategy for makeshift hospitals and public buildings to contain covid-19 and other airborne diseases: Ventilation strategy for covid-19, R. Soc. Open Sci. 7 (9). doi:10.1098/rsos.200680.

[14] A. W. Woods, C. Caulfield, J. C. Phillips, Blocked natural ventilation: The effect of a source mass flux, J. Fluid Mech. 495 (2003) 119 – 133. doi:10.1017/S0022112003005627.

[15] A. S. Kuesters, A. W. Woods, The formation and evolution of stratification during transient mixing ventilation, J. Fluid Mech. 670 (2011) 66 – 84. doi:10.1017/S0022112010005392.

[16] N. Kaye, G. Hunt, Overturning in a filling box, J. Fluid Mech. 576 (2007) 297 – 323. doi:10.1017/S0022112006004435.

[17] I. Coomaraswamy, C. Caulfield, Time-dependent ventilation flows driven by opposing wind and buoyancy, J. Fluid Mech. 672 (2011) 33–59. doi:10.1017/S0022112010005847.

[18] J. Craske, G. O. Hughes, On the robustness of emptying filling boxes to sudden changes in the wind, J. Fluid Mech. 868 (2019) R3. doi:10.1017/jfm.2019.199.

[19] N. Kaye, G. Hunt, Time-dependent flows in an emptying filling box, J. Fluid Mech. 520 (2004) 135 – 156. doi:10.1017/S0022112004001156.

[20] B. Lishman, A. W. Woods, On transitions in natural ventilation flow driven by changes in the wind, Build. Environ. 44 (4) (2009) 666 – 673. doi:10.1016/j.buildenv.2008.05.012.

[21] B. Lishman, A. W. Woods, The effect of gradual changes in wind speed or heat load on natural ventilation in a thermally massive building, Build. Environ. 44 (4) (2009) 762 – 772. doi:10.1016/j.buildenv.2008.06.026.

[22] G. Lane-Serff, S. Sandbach, Emptying non-adiabatic filling boxes: The effects of heat transfers on the fluid dynamics of natural ventilation, J. Fluid Mech. 701 (2012) 386 – 406. doi:10.1017/jfm.2012.164.

[23] F. Durrani, M. J. Cook, J. J. McGuirk, Evaluation of les and rans cfd modelling of multiple steady states in natural ventilation, Build. Environ. 92 (2015) 167 – 181. doi:10.1016/j.buildenv.2015.04.027.

[24] P. Heiselberg, Y. Li, A. Andersen, M. Bjerre, Z. Chen, Experimental and cfd evidence of multiple solutions in a naturally ventilated building, Indoor Air 14 (1) (2004) 43 – 54. doi:10.1046/j.1600-0668.2003.00209.x.

[25] J. L. Partridge, P. Linden, Validity of thermally-driven small-scale ventilated filling box models, Exp. Fluids 54 (11). doi:10.1007/s00348-013-1613-4.

[26] A. D. Stavridou, P. E. Prinos, Natural ventilation of buildings due to buoyancy assisted by wind: Investigating cross ventilation with computational and laboratory simulation, Build. Environ. 66 (2013) 104 – 119. doi:10.1016/j.buildenv.2013.04.011.

[27] R. W. Mott, A. W. Woods, Quasi-steady states in natural displacement ventilation driven by periodic gusting of wind, J. Fluid Mech. 707 (2012) 1 – 23. doi:10.1017/jfm.2012.230.

[28] Y. Li, A. Delsante, Z. Chen, M. Sandberg, A. Andersen, M. Bjerre, P. Heiselberg, Some examples of solution multiplicity in natural ventilation, Build. Environ. 36 (7) (2001) 851 – 858. doi:10.1016/S0360-1323(01)00011-7.

[29] J. Yuan, L. R. Glicksman, Multiple steady states in combined buoyancy and wind driven natural ventilation: The conditions for multiple solutions and the critical point for initial conditions, Build. Environ. 43 (1) (2008) 62 – 69. doi:10.1016/j.buildenv.2006.11.035.

[30] D. Bolster, C. Caulfield, Transients in natural ventilation — a time-periodically-varying source, Build. Serv. Eng. Res. Technol. 29 (2) (2008) 119–135. doi:10.1177/0143624407087849.

[31] D. Bower, C. Caulfield, S. Fitzgerald, A. Woods, Transient ventilation dynamics following a change in strength of a point source of heat, J. Fluid Mech. 614 (2008) 15 – 37. doi:10.1017/S0022112008003479.

[32] P. J. Edwards, R. B. Hurst, Level-crossing statistics of the horizontal wind speed in the planetary surface boundary layer, Chaos 11 (3) (2001) 611 – 618. doi:10.1063/1.1379310.

[33] E. Van Doom, B. Dhruva, K. R. Sreenivasan, V. Cassella, Statistics of wind direction and its increments, Phys. Fluids 12 (6) (2000) 1529 – 1534. doi:10.1063/1.870401.

[34] J. P. Arenas-López, M. Badaoui, Stochastic modelling of wind speeds based on turbulence intensity, Renew. Energy 155 (2020) 10 – 22.

[35] M. Mora-Perez, I. Guillén-Guillamón, P. A. López-Jiménez, Computational analysis of wind interactions for comparing different buildings sites in terms of natural ventilation, Adv. Eng. Software 88 (2015) 73 – 82. doi:10.1016/j.advengsoft.2015.06.003.

[36] L. Ridolfi, P. D'Odorico, F. Laio, Noise-induced phenomena in the environmental sciences, Vol. 9780521198189, 2011. doi:10.1017/CBO9780511984730.

[37] R. Vesipa, C. Camporeale, L. Ridolfi, Noise-driven cooperative dynamics between vegetation and topography in riparian zones, Geophys. Res. Lett. 42 (19) (2015) 8021 – 8030. doi:10.1002/2015GL065688.

[38] R. Vesipa, C. Camporeale, L. Ridolfi, Recovery times of riparian vegetation, Water Resour. Res. 52 (4) (2016) 2934 – 2950. doi:10.1002/2015WR018490.

[39] R. Vesipa, E. Paissoni, C. Manes, L. Ridolfi, Dynamics of bubbles under stochastic pressure forcing, Phys. Rev. E 103 (2). doi:10.1103/PhysRevE.103.023108.

[40] A. Fontanini, U. Vaidya, B. Ganapathysubramanian, A stochastic approach to modeling the dynamics of natural ventilation systems, Energy Build. 63 (2013) 87–97. doi:10.1016/j.enbuild.2013.03.053.

[41] B. R. Morton, G. I. Taylor, J. S. Turner, Turbulent gravitational convection from maintained and instantaneous sources, Proc. Roy. Soc. London A 234 (1956) 1–23.

[42] W. Baines, Turbulent buoyant convection from a source in a confined region, J. Fluid Mech. 37 (1) (1969) 51 – 80. doi:10.1017/S0022112069000413.

[43] G. K. Vallis, Atmospheric and Oceanic Fluid Dynamics: Fundamentals and Large-Scale Circulation, 2nd Edition, Cambridge University Press, 2017. doi:10.1017/9781107588417.

[44] J. Ma, M. Fouladirad, A. Grall, Flexible wind speed generation model: Markov chain with an embedded diffusion process, Energy 164 (2018) 316–328. doi:10.1016/j.energy.2018.08.212.

[45] G. Uhlenbeck, L. Ornstein, On the theory of the brownian motion, Physical Review 36 (5) (1930) 823–841. doi:doi.org/10.1103/PhysRev.36.823.

[46] A. Gu, B. Guo, B. Wang, Long term behavior of random navier-stokes equations driven by colored noise, Discrete Contin. Dyn. Syst. Ser. B 25 (7) (2020) 2495–2532. doi:10.3934/dcdsb.2020020.

[47] G. M. Jónsdóttir, F. Milano, Data-based continuous wind speed models with arbitrary probability distribution and autocorrelation, Renew. Energy 143 (2019) 368 – 376. doi:10.1016/j.renene.2019.04.158.

[48] A. Loukatou, S. Howell, P. Johnson, P. Duck, Stochastic wind speed modelling for estimation of expected wind power output, Appl. Energy 228 (2018) 1328 – 1340. doi:10.1016/j.apenergy.2018.06.117.

[49] R. Zárate-Miñano, M. Anghel, F. Milano, Continuous wind speed models based on stochastic differential equations, Appl. Energy 104 (2013) 42 – 49. doi:10.1016/j.apenergy.2012.10.064.

[50] R. Zarate-Minano, F. M. Mele, F. Milano, Sde-based wind speed models with weibull distribution and exponential autocorrelation, Vol. 2016-November, 2016. doi:10.1109/PESGM.2016.7741754.

[51] D. Gillespie, Exact numerical simulation of the ornstein-uhlenbeck process and its integral, Phys Rev E. 54 (2) (1996) 2084–2091. doi:10.1103/PhysRevE.54.2084.

[52] G. Marsaglia, W. W. Tsang, The ziggurat method for generating random variables, J. Stat. Softw. 5 (8) (2000) 1–7. doi:10.18637/jss.v005.i08.

[53] J. Dormand, P. Prince, A family of embedded runge-kutta formulae, J. Comput. Appl. Math. 6 (1) (1980) 19–26. doi:10.1016/0771-050X(80)90013-3.